SEMARAK ILMU PUBLISHING

Journal of Advanced Research in Numerical Heat Transfer

Journal homepage:
https://semarakilmu.com.my/journals/index.php/arnht/index
ISSN: 2735-0142

Numerical Simulation on the Spray Angle of the Dual-layer Hole Nozzle in a Partition Combustion System of the Diesel Engine

Lu Hongkun[1,2], Muhamad Mat Noor[1,3,*], Li Li[1,4], Kumaran Kadirgama[1]

[1] Faculty of Mechanical & Automotive Engineering Technology, Universiti Malaysia Pahang Al-Sultan Abdullah (UMPSA), Pekan, Pahang, Malaysia
[2] School of Automotive Engineering, Jiujiang Vocational and Technical College, Jiujiang 332000, Jiangxi, China
[3] Centre for Research in Advanced Fluid & Processes, Universiti Malaysia Pahang Al-Sultan Abdullah, Kuantan, Pahang, Malaysia
[4] Faculty of Electrical Engineering, Changchun Automobile Industry College, China

ARTICLE INFO

Article history:
Received 25 January 2024
Received in revised form 20 February 2024
Accepted 22 March 2024
Available online 30 April 2024

Keywords:
Double ω-shaped combustion chamber; double-layer hole nozzle; spray angle; numerical simulation

ABSTRACT

To study the effect of the spray angles of the dual-layer hole nozzle on the combustion and emissions performance in the partition combustion system, the in-cylinder spray, mixture formation and combustion processes of the new combustion system were simulated and investigated using AVL FIRE software. The results show that, compared with the variation of the lower-layer spray angles, the change of the upper-layer spray angles has a great influence on the instantaneous heat release rate. The increasing spray angles of the lower-layer holes lead to reduced peak values of the heat release rate in the cylinder. In all the spray angle cases, the first fire area of the cylinder is in the B zone of the combustion chamber. Compared with lower-layer spray angle, the upper-layer spray angle has a greater impact on the airflow disturbance in the combustion chamber. Appropriately increasing the upper-layer spray angle facilitates the mixing of fuel and air in the combustion chamber and reduces the unburnt fuel equivalence ratio. When the spray angles of the upper- and lower-layer holes are 157° and 112°, respectively, the combustion indicates power has the largest value of 12.18 kW. At the same time, the Soot emission is also the smallest, with a value of 0.52 g/kW·h.

1. Introduction

For the diesel engine, the structure of the combustion chamber significantly influences the in-cylinder airflow, the formation of the air-fuel mixture, and the combustion process [1]. Consequently, optimizing the combustion chamber's configuration is crucial for improving air-fuel mixture formation and optimizing the combustion process [2,3]. Employing cost-effective and straightforward techniques for strategic airflow management can enhance spray spatial distribution, improve air-fuel mixture formation, and facilitate combustion within the combustion chamber [4,5]. This approach is important in reducing fuel consumption and emissions for low-power non-road diesel engines [6].

* *Corresponding author.*
E-mail address: muhamad@umpsa.edu.my (Muhamad Mat Noor)

https://doi.org/10.37934/arnht.19.1.2942

Three-dimensional numerical simulations enhance understanding of complex physical and chemical processes during in-cylinder flow and combustion in internal combustion engines [7,8]. These simulations reveal the influence of combustion system parameters on the combustion process and emissions [9-11]. In this study, the CFD software FIRE was employed to conduct numerical simulations of the proposed combustion system's spray and combustion processes [12]. The research extensively analyzed the effects of changes in the spray angles of double-layer holes nozzle on in-cylinder combustion and emission performance from various perspectives.

2. The partition combustion system

The combustion chamber structure of the diesel engine should facilitate rapid fuel diffusion into the upper region of the chamber, promoting swift mixing with air and accelerating combustion [13]. The core concept of the partition combustion system involves introducing a ridge on the combustion chamber wall, dividing it into two annular regions: an upper zone labeled as Zone A and a lower area marked as Zone B, as depicted in Figure 1. The ridge on the combustion chamber wall intensifies airflow disturbances between zones A and B during the piston's upward and downward movements. Prior to reaching the top dead center (TDC), as the piston ascends, the predominant in-cylinder airflow consists of squish and turbulence, gradually shifting from Zone A towards Zone B [14]. Due to the relatively confined space in Zone B, robust squish motion develops, facilitating fuel-air mixture formation within this zone. After reaching the TDC, under the influence of reverse squish and combustion vortexes, airflow from Zone B streams outward into the space of Zone A during the piston's descent, further enhancing fuel-air mixture within Zone A and promoting combustion.

Taking into account the distinctive shape characteristics of the new combustion chamber in the partition combustion system, an optimized design for a dual-layer hole nozzle with different spray angles has been developed to match the dual-ω-shaped combustion chamber structure [15]. The dual-row hole nozzle exhibits superior fuel spatial distribution properties [16,17]. By altering the number, size, and distribution of the holes in the nozzle, the fuel distribution along the axial direction becomes more adaptable [18]. The fuel streams from the upper- and lower-layer holes of nozzles are directed respectively into zones A and B within the combustion chamber. Modifying the fuel quantities from the upper and lower row holes of nozzle along with adjusting the sizes of Zones A and B within the combustion chamber enhances fuel spatial distribution, improves air utilization efficiency, fosters air-fuel mixture formation, and consequently achieves highly efficient and clean combustion [19].

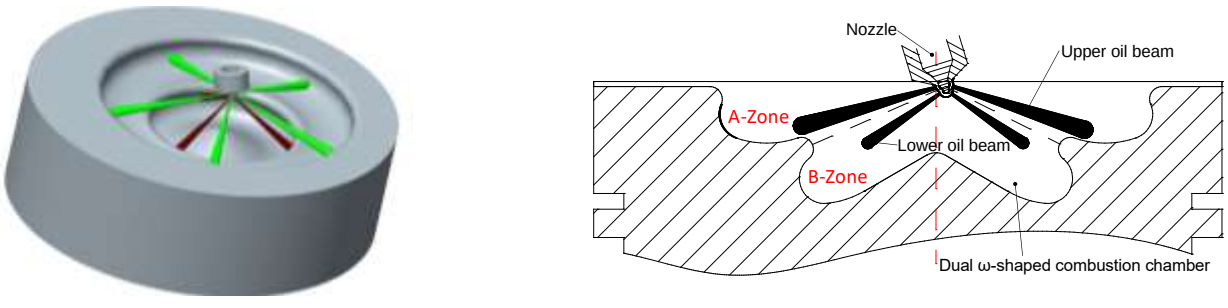

(a) (b)

Fig. 1. Structure schematic diagram of the partition combustion system, a) Three-dimensional space diagram, b) Two-dimensional space diagram

3. Research objects and research methods

3.1 Research Objects

The research focuses on the ZS1100M diesel engine, which is a horizontally oriented, single-cylinder, four-stroke, naturally aspirated, and water-cooled direct injection diesel engine. The original combustion chamber configuration of the engine is an open ω-shaped design. The primary technical specifications of the engine are detailed in Table 1.

Table 1
The main parameters of the diesel engine

Basic items	Diesel engine parameters
Rated speed / (r/min)	2200
Bore size × stroke /mm	100×115
Rated power /kW	11.1
Cylinder working volume /L	0.903
Compression ratio	17.5

The initial conditions, boundary conditions, and relevant parameters utilized in the simulation study are presented in Table 2 [19]. These parameters correspond to the rated load condition of the original engine. The boundary conditions are derived from measured data, while the initial pressure and temperature are based on verified one-dimensional AVL BOOST simulation results [20]. The fuel injection rate is constant, thus maintaining a consistent excess air ratio.

Table 2
The conditions and parameters of the simulation

Basic items	Initial parameters
Initial pressure /MPa	0.09
Initial temperature /K	330
Intake swirl ratio	2.25
Piston temperature /K	523
Cylinder head temperature /K	423
Cylinder liner temperature /K	373
Cycle fuel injection mass /mg	44.0
Injection timing /° CA BTDC	8

3.2 Computational Models and Meshing

This paper employs the k-ζ-f four-equation model for turbulence modeling . The spray breakup utilizes the WAVE model, while collision employs the Naber Reitz oil droplet-wall collision model with a Wal1jet1 interaction type, C2=12, a critical Weber number of 50, and reflection angles less than 5°. Oil droplet evaporation relies on the Dukowicz model, ignition uses the Shell auto-ignition model, and combustion is modeled using the ECFM-3Z approach [21]. NO_X emission is estimated using the Zeldovich model, and Soot emission is predicted using the Kennedy-Hiroyasu-Magnussen model [22].

This paper simplifies the combustion system by:

i. Omitting consideration of intake and exhaust strokes, focusing calculations on the interval from the closure of the intake valve to the opening of the exhaust valve. Hence, the geometric model excludes the intake passage, intake valve, exhaust passage, and exhaust valve. The initial conditions are derived from experimental tests.

ii. As the experimental diesel engine's combustion chamber is not machined in the center of the piston crown, the full model is employed for computation.
iii. Compensatory volume was established to ensure consistency in the clearance height and geometric compression ratio with an actual diesel engine.

The entire combustion system model, consisting of hexahedral unstructured grids, is created using the FAME Meshing tool. Sensitivity analysis of grid sizes and simulation time steps is conducted for the combustion chamber, ultimately determining an average grid size of 3.5mm. To account for compression effects during meshing, grids are varied at different crankshaft angles. This approach maintains the aspect ratio of the grids and notably reduces computational load. Grid distributions at different crankshaft angles in this study are depicted in Figure 2, showing approximately 73,008 grids at top dead center and 144,288 grids at bottom dead center.

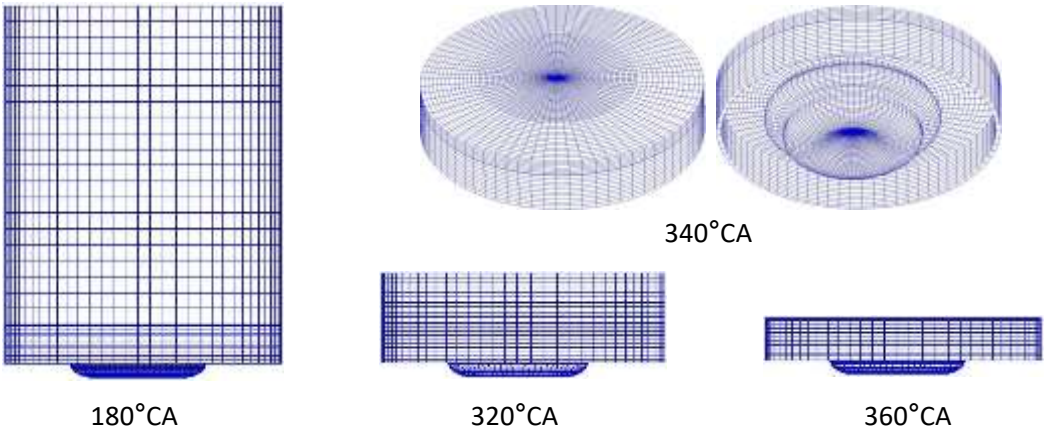

Fig. 2. Mesh model under different crankshaft angles

As demonstrated in Figure 3, the selection settings of various regions within the combustion chamber grids using the FIRE simulation software enable the study of different nozzle spray angles' impacts on airflow and combustion variations within zones A, B, and their intersection region.

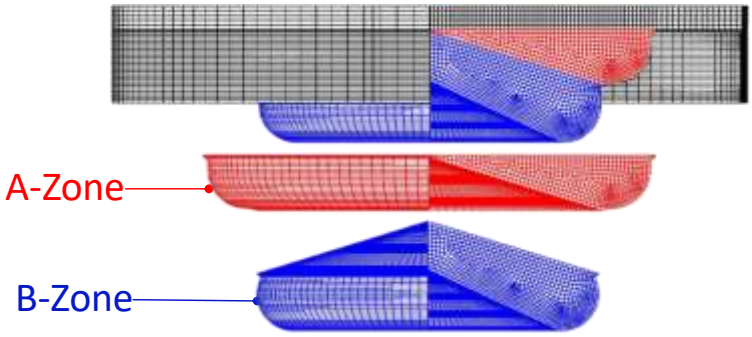

Fig. 3. The regions of A zone and B zone

3.3 Model Validation

To verify the model's accuracy, the simulated cylinder pressure and heat release rate curves are compared with the results from the engine bench test under the original operating conditions [23]. As depicted in Figure 4, the simulation and experimental results of in-cylinder pressure and heat release rate are fundamentally consistent, providing fairly accurate predictions of the cylinder pressure peak and its phase. The discrepancy in cylinder pressure peaks is minimal, with only a

0.03MPa difference, while the phase difference remains within 2°CA. The shape and distribution of the heat release rate curves are substantially similar, with a mere 5J/°CA disparity in the maximum heat release rate peaks. Furthermore, after conversion, the indicated specific energy from 218°CA to 485°CA for the combustion process within the engine stands at 680J according to the original equipment, while the simulated calculation yields 661J, exhibiting a 3% margin of error. This demonstrates that the computational model selected in this study effectively portrays the in-cylinder combustion phenomena of the original engine.

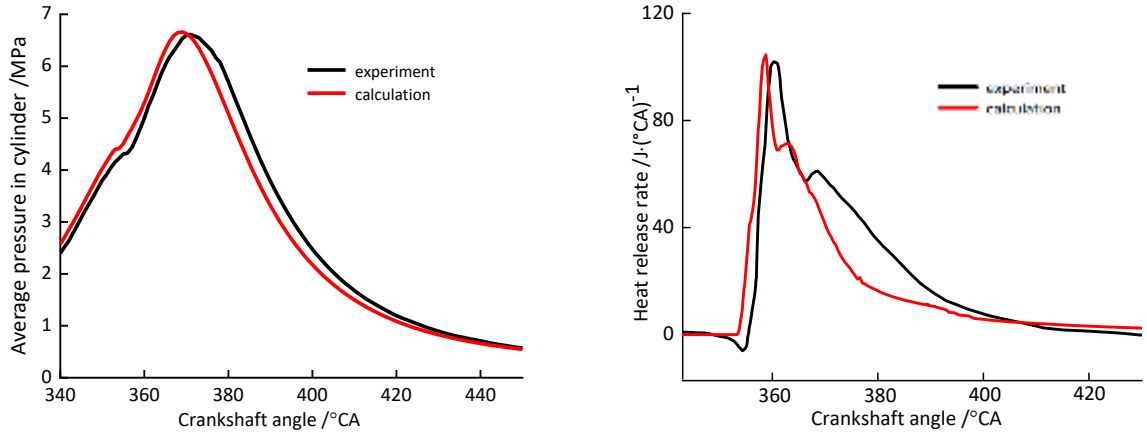

(a) (b)

Fig. 4. Comparison of calculational and experimental results, (a) Average cylinder pressure curves, (b) Heat release rate curves

3.4 Calculation Scheme

In earlier research [15,19], it was discovered that the dual- ω -shaped combustion chambers with smaller throat diameters exhibit superior performance and a distribution of five upper holes and three lower holes nozzle has demonstrated better performance under medium to high loads. The dua- ω -shaped combustion chamber simulated in this study, as depicted in Figure 5(a), maintains a throat diameter identical to that of the original engine, measuring 57mm. Under conditions where the total flow area of the nozzles and the injected fuel volume remain unchanged from the original engine, the configuration employs five upper holes and three lower holes, with diameters of 0.24mm and 0.21mm, respectively. The structural and spatial layout of the nozzle is illustrated in Figure 5(b), where the blue color represents the upper row holes, positioned at an angle α, and the red color represents the lower row holes, set at an angle β.

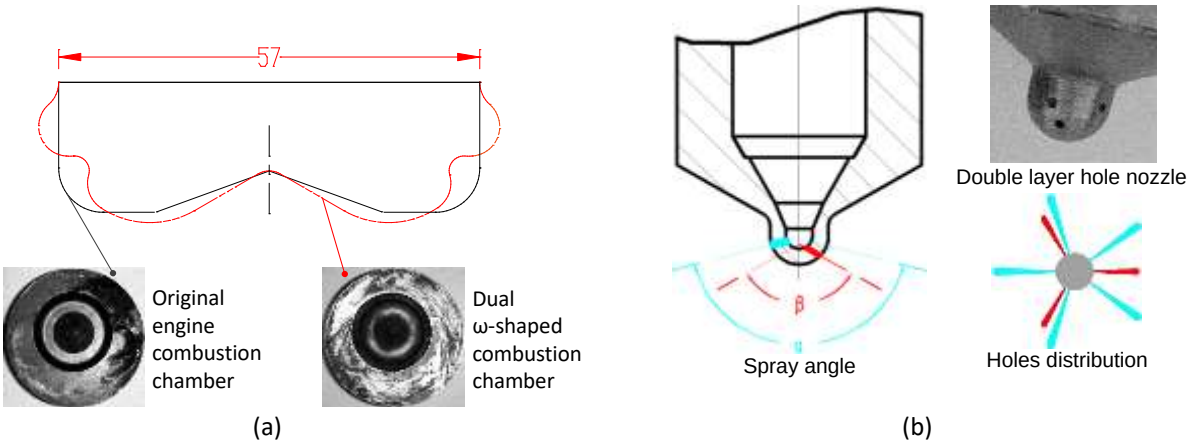

Fig. 5. The combustion chamber and nozzle structure, (a) The combustion chamber structure, (b) The distribution of dual layer holes

To investigate the impact of the spray angles of the dual-row hole nozzle on the combustion and emission performance of the partition combustion system, this study conducted simulations for ten different spray angles cases of the double-layer nozzles. Ensuring that the oil beams emitted from the upper and lower rows of holes fall into the corresponding areas A and B, the specific schemes are detailed in Table 3.

Table 3
Numerical cases

Case No.	Spray angles of upper-layer holes α (°)	Spray angles of lower-layer holes β (°)
Case 1	142	112
Case 2	147	112
Case 3	152	112
Case 4	157	112
Case 5	162	112
Case 6	150	110
Case 7	150	115
Case 8	150	120
Case 9	150	125
Case 10	150	130

4. Result analysis

4.1 Analysis of the heat release rate

The variation in heat release rate can directly reflect the mixing and combustion conditions of gases in the cylinder. Figures 6(a) and 6(b) depict the curves of the instantaneous heat release rate within the cylinder, the proportions of heat release rate in combustion chamber zone A and zone B, corresponding to variations in the spray angles of the upper- and lower-layers holes.

In Figure 6(a), maintaining a fixed spray angle of 112° in the lower row holes while varying the spray angles of the upper row nozzle holes results in substantial changes in the instantaneous heat release rate within the cylinder. When the spray angle of the upper row injector holes increases from 142° to 147°, the peak instantaneous heat release rate within the cylinder rises from 153.8 J/°CA to 170.6 J/°CA, with a corresponding 1°CA phase lag for the peak value. Further increasing the spray angle of upper row holes to 152° leads to a continued rise in the peak instantaneous heat release rate within the cylinder, albeit with a reduced valve of increase, reaching a value of 177.7 J/°CA.

Subsequent increments in the spray angle to 157° and 162° result in a decline in the peak heat release rate, dropping to 153.3 J/°CA and 152.9 J/°CA, respectively. Notably, the heat release rate curves for these angles closely resemble that of the spray angle at 142°, except for the period between 362°CA and 377°CA, where the instantaneous heat release rate within the cylinder is higher than that at the spray angle of 142°.

Correspondingly, as depicted in Figure 6(b), with a constant spray angle of 152° in upper row holes and variation in the spray angles of lower-layer holes, there is minimal variation in the instantaneous heat release rate curve within the cylinder compared with the variation in the spray angles of upper-layer holes. Furthermore, the peak instantaneous heat release rate within the cylinder gradually decreases with an increase in the spray angles, with values of 176.6J/°CA, 175.2J/°CA, 172.8 J/°CA, 166.8J/°CA, and 162.3J/°CA, respectively, with minimal variation in the phase of the peak values concerning the crankshaft angle.

To analyze the mixing and combustion status of fuel-air mixture in different regions of the combustion chamber, a study was conducted on the proportion between the instantaneous local heat release rate $\boldsymbol{q_{zi}}$ in a specified zone of the combustion chamber and the corresponding instantaneous overall heat release rate $\boldsymbol{q_{ti}}$ within the cylinder at that moment. The expression for the proportion of the instantaneous local heat release rate within the specified zone, denoted as ε, is given by the following Eq. (1).

$$\varepsilon = \frac{q_{zi}}{q_{ti}} \times 100\% \tag{1}$$

The paper divides the combustion chamber into zones A and B. It specifically investigates the variation of the ε concerning the combustion of the fuel-air mixture within regions A and B concerning changes in the crankshaft angle when altering the spray angles of the dual-layer holes. It should be noted that when the piston runs near the upper stop, the combustion occurs inside the combustion chamber initially, and at this time the ε in zones A and B is positive. However, as the piston moves down, the burning mixture is taken out of the combustion chamber by the reverse squeezing flow. The ε of zones A and B in the combustion chamber becomes negative, indicating that in the combustion chamber, the combustion is weakened and it is required to absorb additional heat from the other regions of the cylinder to maintain the high temperature.

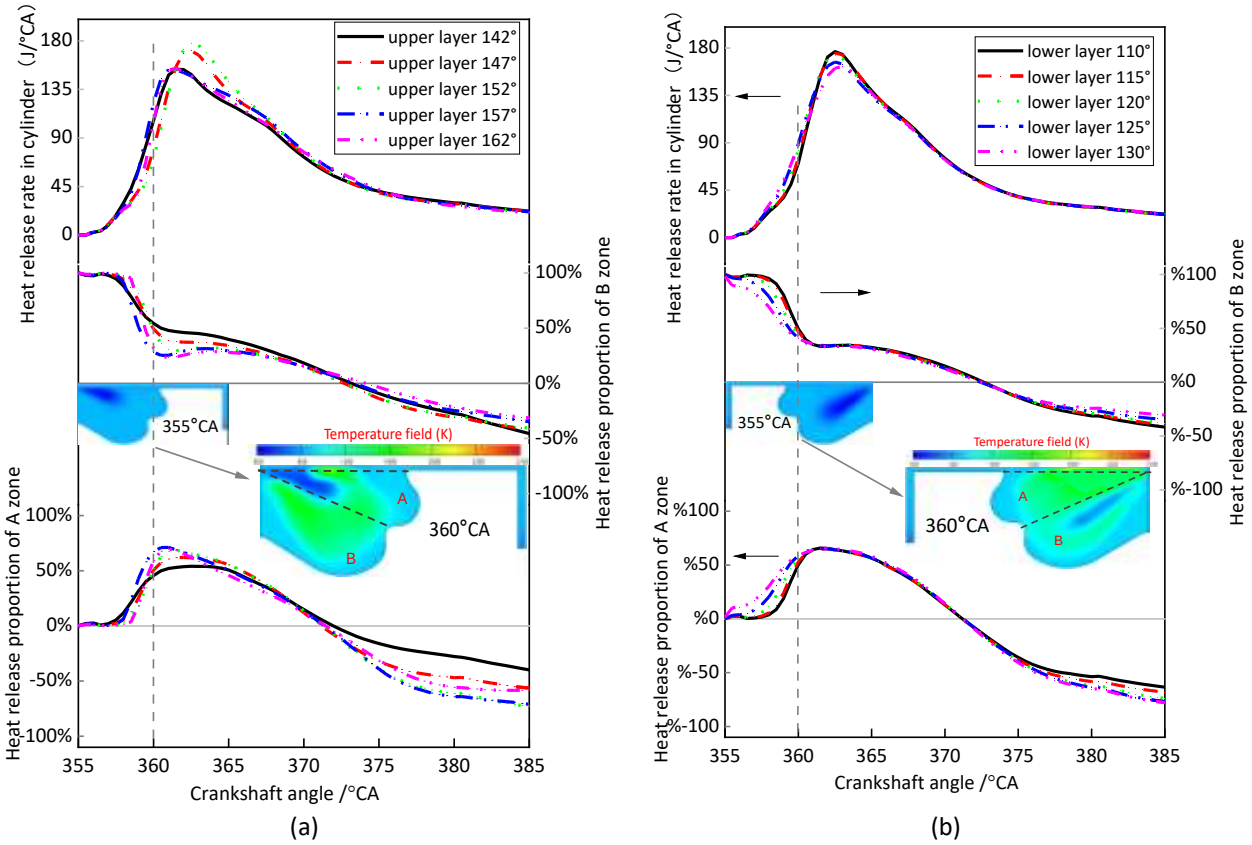

Fig. 6. Heat release rate and the proportion of heat release rate curves in different spray angles, (a) Change of the upper-layer spray angles, (b) Change of lower-layer spray angles

From the curves depicting the instantaneous ε ratio of zones A and B in Figures 6(a) and 6(b), regardless of whether the spray angles of upper or lower-layer holes are modified, it is evident that zone B within the combustion chamber consistently exhibits the earliest ignition and heat release of the mixture gas inside the cylinder, resulting in a heat release ratio close to 1. Subsequently, zone A ignites with a delay, approximately 2°CA later. Once heat release begins in zone A, its heat release ratio increases rapidly, leading to a rapid decrease in the heat release ratio in zone B. It is evident that combustion occurs first on both sides of the oil bundle from the image of the temperature field at 360°CA. In the narrow space of the combustion chamber, the area of maximum combustion in the upper oil bundle is in the B zone, and the area of maximum combustion in the lower oil bundle is in the A zone. After 365°CA, as the piston descends, the mixed flow inside the combustion chamber is displaced outwards, causing the instantaneous heat release ratios in both zones A and B to decrease continuously, eventually reaching negative values. Comparing the corresponding curves in Figures 6(a) and 6(b), it is apparent that as the spray angles of lower-layer holes increases, the ignition timing in zone A advances continuously, and the combustion rate strengthens.

Compared to variations in the spray angles of the lower row holes, alterations in the upper-layer spray angles prompt a rapid decrease in the proportion of instantaneous heat release rate within Zone B, starting from an initial value of 1. Between 360°CA and 365°CA, as the spray angle of the upper row holes increases, the ε within Zone B correspondingly diminishes. However, the rate of reduction gradually lessens. As the piston descends past 370°CA, the ε within Zone A gradually diminishes to negative values. At this point, the differences in ε caused by variations in the spray angle of the upper row holes are greater than those resulting from changes in the spray angle of the upper row holes. The schemes with spray angles of 155° and 160° for the upper row holes exhibit the

highest absolute values for the ε within zone A after 375°CA, indicating that the velocity of fuel-air mixture exiting the Zone A into cylinder is the fastest among all schemes.

4.2 Analysis of the Fuel-Air Mixture Flow Movement

The protruding ridge structure in the partition combustion system is known to enhance airflow disturbances within the combustion chamber [10-12]. To investigate the specific impact of the spray angles on the airflow disturbance in the combustion chamber, this study utilizes software to isolate the intersection surface between zones A and B, obtaining the average flow velocity of the incoming and outgoing airflow at different crankshaft angles. The flow velocity is regarded as positive upon entry into zone A and negative when entering zone B.

Figures 7(a) and 7(b) respectively display the curves of fuel-air mixture flow's average flow velocities within the intersection surface of zones A and B when altering the spray angles of the dual-layer hole nozzle. Overall, regardless of changes in upper- or lower-layers spray angles, before a sharp increase in instantaneous heat release within the cylinder, the airflow movement between zones A and B primarily indicates a flow from zone A to zone B. This demonstrates that the airflow within the combustion chamber is primarily driven by the piston's upward movement causing squeezing at this stage. Post 355°CA, zones B and A sequentially ignite, and the impact of combustion-induced turbulence on the airflow movement inside the cylinder becomes noticeable, leading to a change in the direction of airflow on both sides of the intersection surface. From the velocity field pictures at 360°CA, it can be seen that the upper and lower oil bundles have different effects on the airflow motion at the intersection surface. Since the oil beam of upper raw is close to the intersection surface on the lower side, a disturbance is caused on the intersection surface from zone A to zone B. In contrast, the bundle of lower raw brings a disturbance to the intersection surface from zone B to zone A. As the piston descends, combustion expands outward from the combustion chamber, leading to a continuous decrease in the proportion of combustion occurring within zones B and A. Consequently, from the perspective of the intersection area, airflow during this period (after 365°CA) mainly exits from zone B into zone A.

It's essential to note that in the partition combustion system, during the period about 355°CA - 358°CA, the variations in the upper-layer spray angle have less impact on the airflow movement passing through the intersection surface. However, as the lower-layer spray angle increases, the airflow movement from zone B to zone A tends to decrease.

During the period when the fuel-air mixture is intensely combusted in the combustion chamber (358°CA - 362°CA), there is an increase in the average flow velocity of the mixed entering zone B from zone A, altering the direction of the average flow velocity even at the intersection surface during this period. From the velocity field pictures, it is evident that the significant changes in the flow average velocity passing through the intersection surface during this interval are primarily due to the airflow disturbance caused by the combustion in the A-zone. Consequently, altering the upper-layer spray angle results in substantial changes in the flow movement entering zone B at the intersection surface as the upper-layer spray angle increases. In contrast, varying the lower-layer spray angle has minimal impact on the average flow velocity passing through the intersection surface during this specific period. This is because the airflow disturbance generated by the oil beams of lower row moves in the opposite direction to the reverse squeezing flow produced by the piston's downward movement, and therefore the total mass flow rate through the intersection surface becomes numerically smaller during the period.

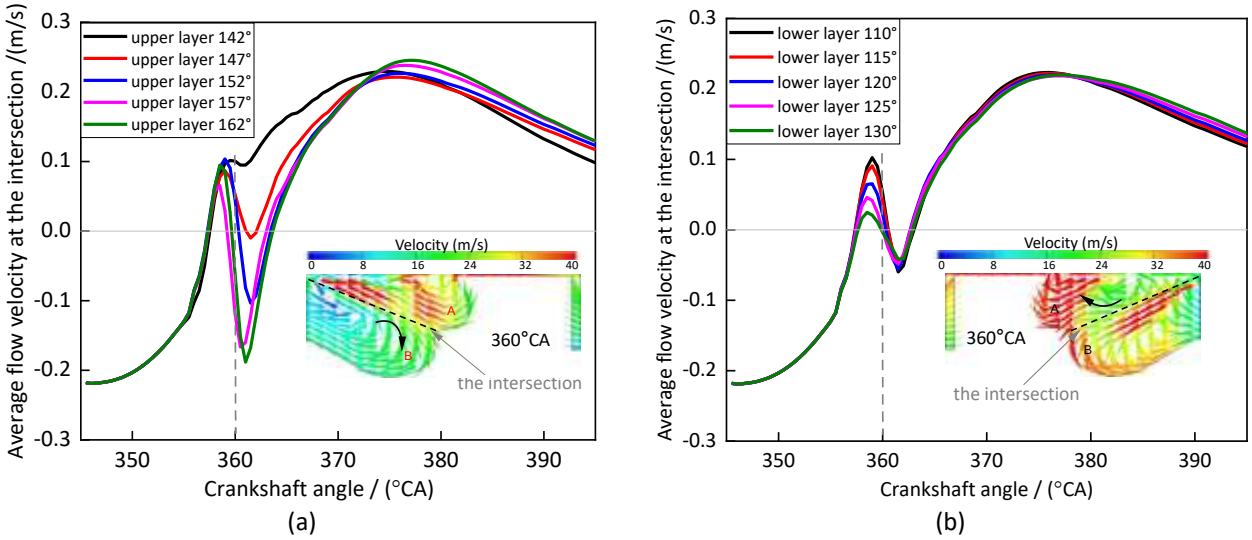

Fig. 7. Average flow velocity curves of the intersection surface in different spray angles, (a) Change of the upper-layer spray angles, (b) Change of lower-layer spray angles

4.3 Analysis of Unburnt Fuel Equivalence Ratio

The unburnt fuel equivalence ratio (ϕ_u) in this paper refers to the equivalence ratio of fuel to air within a specific area at the end of the simulation. The unburnt equivalence ratio is calculated based upon the total mixture mass. The formula is shown in Eq. (2) [11], where $(\frac{A}{F})_{st}$ is the mixing stoichiometric ratio of air to fuel and the unburnt fuel mass fraction y_{fu} is based on the total mixture mass.

$$\phi_u = \frac{y_{fu}}{1-y_{fu}} (\frac{A}{F})_{st} \tag{2}$$

Figure 8 displays the unburnt fuel equivalence ratios in zones A, B, and within the cylinder for various spray angle schemes. When varying the upper-layer spray angles, the unburnt fuel equivalence ratio in zone A drastically reduces from 0.22 to 0.09 as the spray angle increases from 142° to 147°. Further increases in the upper-layer spray angles do not exhibit a distinct pattern in the changes of the unburnt fuel-air equivalence ratio in zone A, and the numerical variations are minor. The unburnt fuel equivalence ratio in zone B continually decreases with the rise in the spray angles, dropping from 0.42 to 0.06. Beyond a spray angle of 152°, the reduction in the unburnt fuel equivalence ratio in zone B becomes less significant. Considering the entire cylinder, an upper-layer spray angle ranging between 142° to 157° results in a noticeable decrease in the unburnt fuel equivalence ratio, reaching its minimum value near 157° at 0.006. Further increases in the spray angle led to an unexpected rise in the unburnt fuel equivalence ratio.

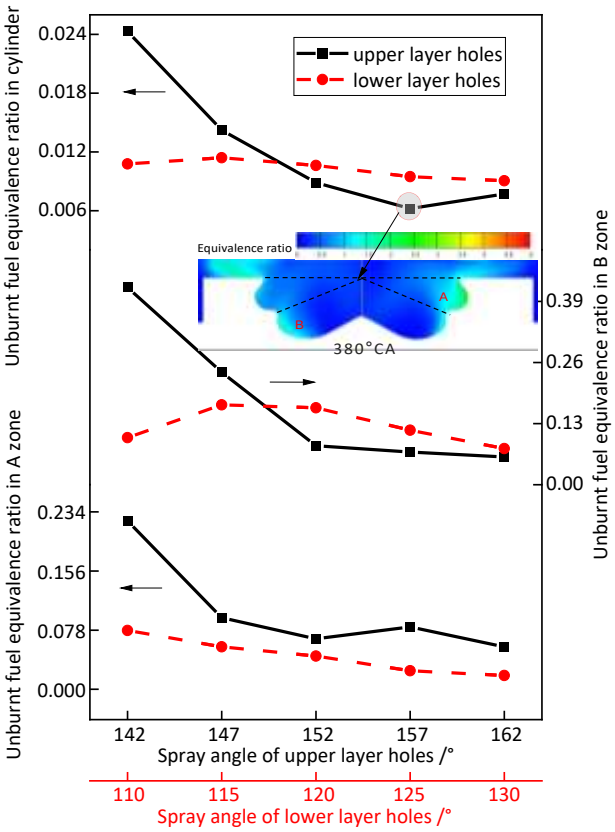

Fig. 8. Unburnt fuel equivalence ratio curves in different spray angles

The effect of varying the lower-layer spray angles on the unburnt fuel equivalence ratio is notably less pronounced than that of varying the upper lower-layer spray angles. As the lower-layer spray angle increases, the unburnt fuel equivalence ratio in zone A steadily decreases, decreasing from 0.08 to 0.02. However, the unburnt fuel equivalence ratio in zone B initially increases and then decreases, reaching its maximum value near 147°. In terms of the unburnt fuel equivalence ratio in the cylinder, increasing the spray angle of lower-layer holes does not significantly impact the reduction of the ratio.

4.4 Analysis of the Indicated Power and Emissions

The paper integrates the computed p-v curve to derive the indicated power and specific emissions at indicated power. The indicated power (kW) serves as an indicator for the combustion performance of the combustion system. The conversion principle involves using the p-v curve to determine the indicated power of the combustion cycle, calculated according to the following Eq. (3).

$$W = \int_{\theta_1}^{\theta_2} \frac{1}{4} p(\theta) \left[2\sin(\theta) + \frac{r\sin(2\theta)}{\sqrt{l^2 - r^2\sin^2(\theta)}} \right] V_h d\theta \tag{3}$$

where p represents the cylinder pressure, l denotes the connecting rod length, r signifies the crank radius, V_h represents the cylinder clearance volume, θ_1 and θ_2 respectively indicate the crank angles corresponding to the intake valve closing and exhaust valve opening. The Eq. (4) corresponds to the indicated power expression.

$$P(kW) = \frac{W(Nm)n(rpm)}{60000z} \tag{4}$$

The computed indicated power from Eq. (4) does not encompass the pumping process. Therefore, the obtained indicated power exhibits certain deviations from the actual values.

As depicted in Figure 9, when altering the spray angles of upper-layer holes between 142° to 157°, the indicated power rises with the spray angle, reaching a peak value of 12.18kW at the spray angle of 157°. Further increasing the spray angles leads to a noticeable decrease in the indicated power. Conversely, concerning the variations in the lower-layer spray angles, the impact on the indicated power is marginal. The indicated power remains relatively constant around 12.0kW with slight fluctuations as the spray angle increases.

In all the cases, as the spray angle increases, the emission of NO increases initially and then decreases. Among the variations in the spray angle of the upper-layer holes, the maximum NO emission occurs at an angle of 157°, measuring 4.16g/kW·h, whereas the minimum NO emission is observed at 162°, measuring 3.73g/kW·h. This indicates that at a spray angle of 157°, the combustion within the cylinder is most intense; further increasing the upper-layer spray angle would lead to deteriorating combustion. Among the alterations in the lower-layer spray angles, the maximum NO emission is observed at an angle of 120°, measuring 4.23g/kW·h, whereas at 110°, the minimum NO emission is recorded at 3.95gkW·h.

The emissions of Soot and NO often exhibit an inverse relationship [24]. The more intense the combustion of the mixed gases within the cylinder, the higher the temperature within the cylinder, leading to the increased NO emissions and decreased Soot emissions. As the spray angle of the upper-layer holes increases, the Soot emission decreases initially and then increases. The lowest Soot emission occurs at a spray angle of 160°, measuring 0.52g/kW·h. When altering the spray angles of the lower-layer holes, the change in the Soot emission remains minimal with an increase in the lower-layer spray angle, maintaining value around 0.55g/kW·h.

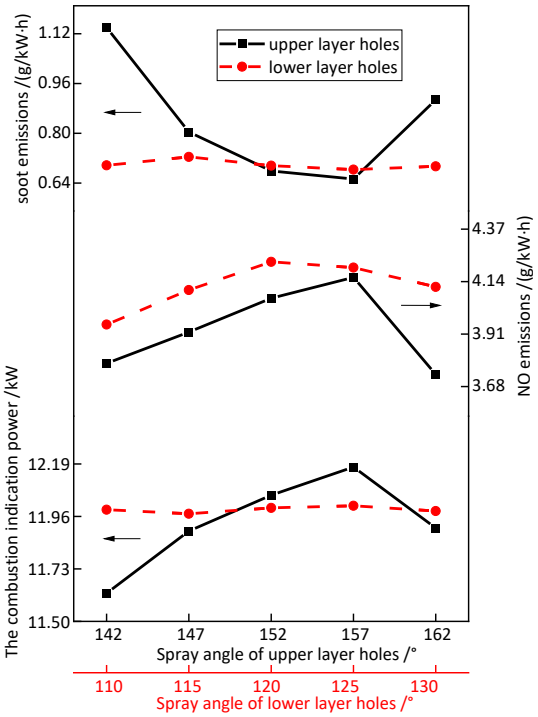

Fig. 9. The combustion indicated power and emissions curves in different spray angles

5. Conclusion

i. When altering the spray angles of the upper-layer holes, there are notable changes in the instantaneous heat release rate curve. At a spray angle of 152°, the cylinder's peak heat release rate was the largest, reaching 177.7J/°CA. Variation in the lower-layer spray angle results in a gradual decrease in the peak instantaneous heat release rate as the spray angle of the lower-layer holes increases.

ii. Regardless of altering the spray angles of the upper- or lower-layers holes, the initial ignition zone within the cylinder is consistently in zone B of the combustion chamber. Changing the spray angle can significantly affect the airflow movement in the combustion chamber. An appropriate elevation of the upper-layer spray angle enhances fuel and air mixing within the combustion chamber, thereby expediting the combustion process.

iii. The impact of altering the spray angles of the lower-layer holes on the unburnt fuel equivalence ratio is notably less pronounced compared to altering the spray angles of the upper-layer holes. During adjustments to the upper-layer spray angles, the unburnt fuel equivalence ratio in the cylinder reaches its minimum value near a spray angle of 157°, measuring 0.006.

iv. At a lower-layer spray angle of 112°, the combustion indicated power reaches its peak at an upper orifice spray angle of 157°, measuring a maximum of 12.18 kW. Concurrently, the emission of Soot is at its minimum, measuring 0.52g/kW·h.

Acknowledgement

This research was funded by a grant from Ministry of Higher Education of Malaysia (FRGS Grant R.J130000.7824.4X172).

References

[1] Temizer, Ilker, and Omer Cihan. "An experimental investigation of new chamber geometry on the combustion characteristics, performance and emissions in a light-duty diesel engine." *Fuel* 345 (2023): 128160. https://doi.org/10.1016/j.fuel.2023.128160

[2] Agarwal, Avinash Kumar, Akhilendra Pratap Singh, and Rakesh Kumar Maurya. "Evolution, challenges and path forward for low temperature combustion engines." *Progress in energy and combustion science* 61 (2017): 1-56. https://doi.org/10.1016/j.pecs.2017.02.001

[3] Maricq, M. Matti. "Engine, aftertreatment, fuel quality and non-tailpipe achievements to lower gasoline vehicle PM emissions: Literature review and future prospects." *Science of The Total Environment* 866 (2023): 161225. https://doi.org/10.1016/j.scitotenv.2022.161225

[4] Deng, Xiwen, Jilin Lei, Jun Wen, Zhigao Wen, and Lizhong Shen. "Influences of piston structural parameters on heat transfer and temperature field of diesel engine piston." *Transactions of the Chinese Society of Agricultural Engineering* 33, no. 10 (2017): 102-108. https://doi.org/10.11975/j.issn.1002-6819.2017.10.013

[5] Moses, Larry Sundaran, Md Tasyrif Abdul Rahman, Abdul Hamid Adom, Mohd Ridzuan Mohd Jamir, Mohd Al Hafiz Mohd Nawi, and Mohd Hafif Basha. "An Analysis of The Material and Design of an Exhaust Manifold for A Single-Cylinder Internal Combustion Engine." *Journal of Advanced Research in Applied Sciences and Engineering Technology* 30, no. 2 (2023): 163-175. https://doi.org/10.37934/araset.30.2.163175

[6] Qian, Yejian, Zhen Gong, Xiaowei Shao, Changfa Tao, and Yuan Zhuang. "Numerical study of the effect of combustion chamber structure on scavenging process in a boosted GDI engine." *Energy* 168 (2019): 9-29. https://doi.org/10.1016/j.energy.2018.11.080

[7] Raman, Venkat, and Malik Hassanaly. "Emerging trends in numerical simulations of combustion systems." *Proceedings of the Combustion Institute* 37, no. 2 (2019): 2073-2089. https://doi.org/10.1016/j.proci.2018.07.121

[8] Pathak, Bhavesh, Asfakahemad Shekh, Nikul Patel, and Vimal Patel. "Review Analysis on CFD Techniques and Numerical Methods for IC Engines Fueled with Diesel and Biofuels." *Journal of Advanced Research in Fluid Mechanics and Thermal Sciences* 110, no. 1 (2023): 40-62. https://doi.org/10.37934/arfmts.110.1.4062.

[9] Zhou, Xinyi, Tie Li, Yijie Wei, and Sichen Wu. "Scaling spray combustion processes in marine low-speed diesel engines." *Fuel* 258 (2019): 116133. https://doi.org/10.1016/j.fuel.2019.116133
[10] Calik, Alper Tolga, Ozgur Oguz Taskiran, and Rafig Mehdiyev. "Numerical investigation of twin swirl application in diesel engine combustion." *Fuel* 224 (2018): 101-110. https://doi.org/10.1016/j.fuel.2018.03.049
[11] Zhang, Zhicheng, Shengli Wei, Jie Chen, Xianyin Leng, Shaobang Zhang, and Shidong Ni. "Numerical Study of the Mixture Formation and Combustion Characteristics in Gasoline Direct Injection Engines with Conical Spray." *Arabian Journal for Science and Engineering* 48, no. 9 (2023): 11525-11535. https://doi.org/10.1007/s13369-022-07492-z
[12] FIRE, AVL. "Users manual." AVL List GmbH, Graz (Austria). Version (2019).
[13] Doppalapudi, Arun Teja, A. K. Azad, and M. M. K. Khan. "Combustion chamber modifications to improve diesel engine performance and reduce emissions: A review." *Renewable and Sustainable Energy Reviews* 152 (2021): 111683. https://doi.org/10.1016/j.rser.2021.111683
[14] Wei, Sheng-Li, Hong-Kun Lu, and Xian-Yin Leng. "Numerical simulation of impinging convexity on partition combustion system performance of diesel engines." *Journal of Jiangsu University: Natural Science Editions* 36, no. 5 (2015): 509-515. https://doi.org/10.3969/j.issn.1671-7775.2015.05.003
[15] Wei, Shengli, Zhiqing Yu, Zhilei Song, Fan Yang, and Chengcheng Wu. "Effect of conical spray and multi-hole spray on gasoline engine mixture formation and combustion performance based on different injection strategies." *Journal of Energy Resources Technology* 143, no. 6 (2021): 062305. https://doi.org/10.1115/1.4048595
[16] Feng, Shiquan, Shenglong Zhang, Hongmei Zhang, and Jidong Shi. "Effect of nozzle geometry on combustion of a diesel-methanol dual-fuel direct injection engine." *Fuel* 357 (2024): 129734. https://doi.org/10.1016/j.fuel.2023.129734
[17] Zhou, Haiqin, Xiangrong Li, Yanlin Chen, Yuning Kang, Dong Liu, and Fushui Liu. "The effect of spray angle on the combustion and emission performance of a separated swirl combustion system in a diesel engine." *Energy* 190 (2020): 116481. https://doi.org/10.1016/j.energy.2019.116481
[18] Guo, Qiang, Jie Liu, Binyang Wu, and Yize Liu. "The multi-parameter optimization of injections on double-layer diesel engines based on genetic algorithm." *Fuel* 339 (2023): 126920. https://doi.org/10.1016/j.fuel.2022.126920
[19] WEI, Sheng-li, Hong-kun LU, Xian-yin LENG, Yu LIANG, Liang CHEN, and Fei-hu WANG. "Experimental Research on Combustion System with Double ω Combustion Chamber for ZS1100M Diesel Engine." *Acta Armamentarii* 37, no. 1 (2016): 17. https://doi.org/10.3969/j.issn.1000-1093.2016.01.003
[20] Lešnik, Luka, Jurij Iljaž, Aleš Hribernik, and Breda Kegl. "Numerical and experimental study of combustion, performance and emission characteristics of a heavy-duty DI diesel engine running on diesel, biodiesel and their blends." *Energy Conversion and Management* 81 (2014): 534-546. https://doi.org/10.1016/j.enconman.2014.02.039
[21] Dayal, Akash, Manish Shrivastava, Rajiv Upadhyaya, and Lakhbir Singh Brar. "Numerical study using detailed chemistry combustion comparing effects of wall heat transfer models for compression ignition diesel engine." *SN Applied Sciences* 1 (2019): 1-6. https://doi.org/10.1007/s42452-019-1033-z
[22] Koten, Hasan. "Investigation of diesel engine performance and emissions by multi-dimensional modeling." *International Journal of Automotive Engineering and Technologies* 7, no. 2 (2018): 76-87. https://doi.org/10.18245/ijaet.458898
[23] WEI, Sheng-li, Fei-hu WANG, Huan CHEN, and Xian-yin LENG. "Research on Effect of Nozzle Hole Distribution on Performance of Combustion System with Double ω CombustionChamber for Diesel Engine." *Acta Armamentarii* 36, no. 1 (2015): 33. https://doi.org/10.3969/j.issn.1000-1093.2015.01.005
[24] Jena, Ashutosh, Akhilendra Pratap Singh, and Avinash Kumar Agarwal. "Optical and computational investigations of the effect of Spray-Swirl interactions on autoignition and soot formation in a compression ignition engine fuelled by Diesel, dieseline and diesohol." *Applied Energy* 324 (2022): 119677. https://doi.org/10.1016/j.apenergy.2022.119677